arXiv:1502.07631v2 [physics.flu-dyn] 18 Mar 2015

The decay of wall-bounded MHD turbulence at low Rm

KACPER KORNET AND ALBAN POTHÉRAT†

Applied Mathematics Research Centre, Coventry University, Coventry, CV51FB, UK

(Received ?; revised ?; accepted ?. - To be entered by editorial office)

We present Direct Numerical Simulations of decaying Magnetohydrodynamic (MHD) turbulence at low magnetic Reynolds number. The domain considered is bounded by periodic boundary conditions in the two directions perpendicular to the magnetic field and by two plane Hartmann walls in the third direction. High magnetic fields (Hartmann number of up to 896) are considered thanks to a numerical method based on a spectral code using the eigenvectors of the dissipation operator. It is found that the decay proceeds through two phases: first, energy and integral lengthscales vary rapidly during a two-dimensionalisation phase extending over about one Hartmann friction time. During this phase, the evolution of the former appears significantly more impeded by the presence of walls than that of the latter. Once the large scales are close to quasi-two dimensional, the decay results from the competition of a two-dimensional dynamics driven by dissipation in the Hartmann boundary layers and the three-dimensional dynamics of smaller scales. In the later stages of the decay, three-dimensionality subsists under the form of barrel-shaped structures. A purely quasi-two dimensional decay dominated by friction in the Hartmann layers is not reached, because of residual dissipation in the bulk. However, this dissipation is not generated by the three-dimensionality that subsists, but by residual viscous friction due to horizontal velocity gradients. Also, the energy in the velocity component aligned with the magnetic field is found to be strongly suppressed, as is transport in this direction. This results reproduces the experimental findings of Kolesnikov & Tsinober (1974).

Key words: Low Rm Magnetohydrodynamics, freely decaying turbulence, turbulence dimensionality, vortex dynamics, two-dimensional turbulence, quasi-two dimensional flows.

1. Introduction

This work concerns the decay of MagnetoHydroDynamic turbulence in electrically conducting fluids subjected to an externally imposed magnetic field. We are particularly interested in the influence of solid, electrically insulating walls on this process. This generic problem is relevant to a number of practical engineering problems in the metallurgy and nuclear industry, but also bears relevance to some aspects of the dynamics of liquid planetary cores and the associated dynamo problem.

When the magnetic field $B\mathbf{e}_z$ is imposed (in the sense of the low magnetic Reynolds number approximation (Roberts (1967)), turbulence evolves as a result of the competition between inertia and the diffusion of momentum along the direction of the magnetic field. A structure of size $l_\perp$ becomes elongated over a length l_z by this diffusion over a timescale

† Email address for correspondence: alban.potherat@coventry.ac.uk

of $\tau_J(l_z/l_\perp)^2$ (Sommeria & Moreau (1982)), whilst loosing energy through Joule dissipation ($\tau_J = \rho/(\sigma B^2)$ is the Joule dissipation time, ρ and σ are the fluid density and electric conductivity.). Moffatt (1967) first showed that under this linear phenomenology, the turbulent kinetic energy decayed at $E \sim t^{-1/2}$ towards an asymptotic state where the flow quantities did not vary along the magnetic field (in this sense,a *two-dimensional* state) but where the kinetic energy of the component along the magnetic field was a third of the total kinetic energy (for a three-component flow). This phenomenology was recovered by Schumann (1976): this author conducted low-resolution direct numerical simulations to confirm that this linear phenomenology applied during less than τ_J but that non-linear effects subsequently led to a decay of the kinetic energy associated to the velocity along $\mathbf{B}$. However, he also found that the skewness tended to a finite value in the later stages of the decay, which he attributed to the persistence of transport of kinetic energy $\mathbf{B}$. The more recent and higher resolution simulations of Burattini *et al.* (2010), confirmed Schumann's findings. Both studies analysed cases where interaction parameter $N = \tau_U/\tau_J$ spanned a range between 0.1 and 50 ($\tau_U(l) = l/U(l_0)$ is the eddy turnover time based on the initial size and velocity of the large scales l_0 and $U(l_0)$). Using the invariance of the "parallel" component of Loitsyansky's integral $I_\parallel$, Okamoto *et al.* (2010) showed that for $N >> 1$, the $t^{-1/2}$ law for the decay of kinetic energy was recovered and that the integral lengthscale in the direction of the magnetic field evolved as $l_z \sim t^{1/2}$. At moderate values of N, a similar approach led the authors to conclude that energy decayed as $E \sim t^{-11/7}$ while the integral lengthscales along and across the magnetic field increased respectively as $l_z \sim t^{5/7}$ and $l_\perp \sim t^{3/14}$. These theoretical scalings as well as the invariance of $I_\parallel$ were verified by means of direct numerical simulations at the highest resolution available to date (up to 2048^3), for $N < 1$.

Aside of inertia, a second major factor is likely to interfere with Moffatt's linear theory: the presence of walls, and in particular Hartmann walls, that are perpendicular to the magnetic field. These are indeed a feature of practically any of the situations where low Rm MHD turbulence is likely to be found. A strictly two-dimensional state is not possible in their presence because of the very thin Hartmann boundary layers that develop along them (see for instance Moreau (1990)). Instead, Sommeria & Moreau (1982) theorised that in a channel of width L, a structure of size $l_\perp$ became quasi-two-dimensional after $\tau_{2D}(l_\perp) \sim \tau_J(L/l_\perp)^2$. Past this stage, electric current in the core became of order Ha^{-1}, the ratio of the boundary layer thickness to L: dissipation occurs then almost exclusively in the boundary layers and is equally viscous and magnetic. In contrast, strictly two-dimensional states are possible when walls are absent and the Joule dissipation can therefore drop to much lower values. Kolesnikov & Tsinober (1974) also observed experimentally that in the presence of Hartmann walls, transport along the magnetic field was suppressed in the later stages of the decay. This was interpreted as an evidence of suppression of the velocity component in this direction, in contrast to the prediction of theories and simulations where no wall was present. Nevertheless, although a "through" velocity component is precluded by the walls, Ekman pumping can still potentially lead to strong vertical velocities at moderate N (Pothérat *et al.* 2000). More recently, it was also found that even for $N > 1$, a small amount of three-dimensionality could lead to a complex system of three-dimensional co- and contrarotating recirculations (Pothérat *et al.* 2013; Baker *et al.* 2015).

Until recently, numerically simulating MHD turbulence at high N in the presence of walls incurred prohibitive computational costs because of the need to resolve the Hartmann boundary layers. Recently, the authors took a different approach to the simulation of these flows based on spectral methods using bases of functions whose elements already

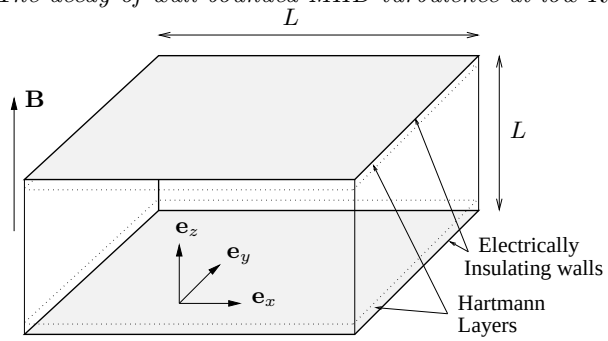


FIGURE 1. Geometry of the Channel flow with transverse magnetic field

incorporate these layers. These partly alleviate this computational constraint to the point where the computational cost becomes independent of *Ha* (Dymkou & Pothérat (2009); Kornet & Pothérat (2014)). We propose to take advantage of this new technique to investigate decaying turbulence in a channel bounded by electrically insulating walls in view of answering the following questions.

(*a*) Does three-dimensionality subsist in the later stages of the decay ($t >> \tau_{2D}(l_\perp)$)?
(*b*) Which part of the energy subsists in the third velocity component ?
(*c*) How do Hartmann walls affect the early phases of the decay ($t < \tau_{2D}(l_\perp)$) ?

We shall first recall the governing equations and the timescales that govern the problem (section 2). Our numerical method and simulation strategy is presented in section 3. We then examine the earlier decay phase which is expected to present the strongest similarities with earlier works not involving walls (section 4). The later stages of the decay where similarities with two-dimensional turbulence are expected are analysed in section 5. The robustness of our results is tested in section 6 by changing initial conditions and domain size.

2. Governing equations

2.1. *Problem definition*

At low Magnetic Reynolds number, the full system of the induction equation and the Navier-Stokes equations for an incompressible fluid can be approximated to the first order (The Magnetic Reynolds number *Rm* represents the ratio of the induced magnetic field to the imposed one). This leads to the following system (Roberts 1967):

$$\frac{\partial \mathbf{u}}{\partial t} + (\mathbf{u}\cdot\nabla)\mathbf{u} = -\frac{1}{\rho}\nabla p + \nu\Delta\mathbf{u} + \frac{1}{\rho}\mathbf{j}\times\mathbf{B}\,, \tag{2.1}$$

$$\nabla\cdot\mathbf{u} = 0\,, \tag{2.2}$$

$$\nabla\cdot\mathbf{j} = 0\,, \tag{2.3}$$

$$\mathbf{j} = \sigma(-\nabla\Phi + \mathbf{u}\times\mathbf{B})\,, \tag{2.4}$$

where $\mathbf{u}$ denotes fluid velocity, $\mathbf{B}$ - externally imposed magnetic field, $\mathbf{j}$ - electric current density, ν - kinematic viscosity, σ - electrical conductivity, Φ - electric potential. We consider a channel flow with a homogeneous transverse magnetic field $B\mathbf{e}_z$ and impermeable ($\mathbf{u}|_{wall} = \mathbf{0}$), electrically insulating ($\mathbf{j}\cdot\mathbf{n}|_{wall} = \mathbf{0}$) walls located at $z = \pm L/2$ (see fig. 1). In the xy directions we impose periodic boundary conditions with period L. Following Roberts (1967), the Lorentz force can be expressed as the sum of a gradient of magnetic pressure p_m and a rotational term:

$$\mathbf{j}\times\mathbf{B} = -\nabla p_m - \sigma B^2 \Delta^{-1}\partial_{zz}\mathbf{u}. \tag{2.5}$$

Using the above identity and adopting the reference scale L, time L^2/ν and velocity ν/L the set of equations (2.1-2.4) can be expressed in dimensionless form:

$$\frac{\partial \mathbf{u}}{\partial t} + P[(\mathbf{u}\cdot\nabla)\mathbf{u}] = \Delta\mathbf{u} - \frac{1}{Ha^2}\Delta^{-1}\partial_{zz}\mathbf{u}\,, \tag{2.6}$$

where $Ha = LB\sqrt{\sigma/\rho\nu}$ is the Hartman number and P denotes orthogonal projection onto the subspace of solenoidal fields.

2.2. *Timescales of the decay*

We now consider an initially turbulent, isotropic flow, left to decay from $t = 0$ under the action of the Lorentz force and viscous friction, in the configuration described above. Hartmann walls can be expected to exert little influence on the initial phase of the decay, during which strong two-dimensionalisation of the flow should take place, as in the simulations of Schumann (1976); Okamoto *et al.* (2010) and others. Unlike, in this previous studies, the presence of physical walls may lead to a physically realistic phase beyond this initial one, where the flow dynamics may become a two-dimensional to some extent. To obtain a first estimate for the timescale for the transition between these two phases, let us first consider a single turbulent structure of size $l_\perp$, which diffuses across the channel width L under the action of the Lorentz force in time $\tau_{2D}(l_\perp) = \tau_J(L/l_\perp)^2$. If this timescale is shorter than both the inertial timescale $\tau_U(l_\perp) = l_\perp/U(l_\perp)$ and the viscous timescale $\tau_\nu(l_\perp) = \nu/l_\perp^2$, then this single structure is quasi-two-dimensional. Two conditions for two-dimensionality ensue:

$$\left(\frac{l_\perp}{L}\right)^3 > \frac{l_0}{L}\frac{U(l_\perp)}{U(l_0)}\frac{1}{N(l_0)}, \tag{2.7}$$

$$\left(\frac{l_\perp}{L}\right)^2 > \frac{1}{Ha}, \tag{2.8}$$

where l_0 denotes the size of the large scales at $t = 0$. Since both these conditions are scale-dependent, each of them defines a minimum two-dimensional scale. Consequently, in a turbulent flow where $N = \tau_U(l_\perp)/\tau_J >> 1$, larger scales are two-dimensional while smaller scales may still be three-dimensional. From inertial condition (2.7), the smallest quasi-two-dimensional structure satisfies $l_\perp^{2D} \sim L[(l_0 U(l_\perp^{2D})/(N(l_0)LU(l_0))]^{1/3}$. Since the two-dimensionalisation time $\tau_{2D}(l_\perp)$ increases with $l_\perp$, this scale is also the slowest structure to become two-dimensional and so $\tau_{2D}^M = \tau_{2D}(l_\perp^{2D})$ provides an estimate for the two-dimensionalisation phase:

$$\tau_{2D}^M \sim \tau_J \left(N(l_0)\frac{U(l_0)h}{U(l_\perp^{2D})l_0}\right)^{2/3}. \tag{2.9}$$

τ_{2D}^M depends on $U(l_\perp^{2D})$, which is expected to drop by several orders of magnitudes during the two-dimensionalisation phase. Not only does this variation of $U(l_\perp^{2D})$ considerably slow down two-dimensionalisation at the initial scale $l_\perp^{2D}(t = 0)$, but scales smaller than the initial value of $l_\perp^{2D}$ may satisfy (2.7) and may in turn become quasi-two-dimensional in a time significantly longer than the initial value of (2.9). On these grounds, a lower estimate for the two-dimensionalisation time is obtained by evaluating (2.9) based on the value of $U(l_\perp)$ at $t = 0$ (this value is fixed by the choice of initial turbulent spectrum).

From viscous condition (2.8), by contrast, the smallest quasi-two-dimensional scale $l_\perp^{2D}$

does not depend on $U(l_\perp)$, and neither does the associated two-dimensionalisation time:

$$l_\perp^{2D} \sim LHa^{-1/2} \tag{2.10}$$

$$\tau_{2D}^M = \tau_{2D}(l_\perp^{2D}) \sim \tau_J Ha^{-1} = \tau_H \tag{2.11}$$

Since no scale smaller than (2.11) can become two-dimensional regardless of how much turbulent intensity drops, τ_H represents a closer estimate of the timescale for two-dimensionalisation of the whole turbulent flow than (2.9).

2.3. *Two-dimensional decay*

Once all structures have become quasi two-dimensional, the evolution of the flow is governed by two-dimensional dynamics with an added friction due to the Hartmann layers. Sommeria & Moreau (1982) showed that the velocity averaged across the channel $\bar{\mathbf{u}} = \int_{-1}^{1} \mathbf{u}_\perp dz$ satisfied a shallow water equation of the form:

$$\frac{\partial \bar{\mathbf{u}}}{\partial t} + (\bar{\mathbf{u}} \cdot \nabla_\perp)\bar{\mathbf{u}} = -\frac{1}{\rho}\nabla_\perp p + \nu \Delta_\perp \bar{\mathbf{u}} - \frac{2\bar{\mathbf{u}}}{\tau_H}\,, \tag{2.12}$$

$$\nabla_\perp \cdot \bar{\mathbf{u}} = 0, \tag{2.13}$$

where operators with subscript $\perp$ operate in the x-y plane only. τ_H appears as the typical time for the dissipation due to the Hartmann boundary layers, and therefore a characteristic time of the two-dimensional dynamics. From (2.12), the evolution of the total kinetic energy $E \simeq E_{2D} = \|\bar{\mathbf{u}}\|_2^2$ associated to the mean flow $\bar{\mathbf{u}}$ when the flow follows a two-dimensional dynamics reduces to

$$\frac{1}{2}\frac{dE_{2D}}{dt} = -2\frac{E_{2D}}{\tau_H} - \nu \|\nabla \bar{\mathbf{u}}\|_{2D}^2, \tag{2.14}$$

where $\|\cdot|_{2D}$ represents the two-dimensional $\mathcal{L}^2$ norm. Introducing lengthscale $l_\perp^\nu = (\|\bar{\mathbf{u}}\|_{2D}^2/\|\nabla\bar{\mathbf{u}}\|_{2D}^2)^{1/2}$ which characterises velocity gradients in the (x, y) plane, it comes that

$$\frac{dE_{2D}}{dt} = -\frac{4}{\tau_H}\left[1 + \frac{1}{2Ha}\left(\frac{L}{l_\perp^\nu}\right)^2\right] E_{2D}. \tag{2.15}$$

It follows from the respective definitions of the total kinetic energy E and E_{2D}, that

$$E = E_{2D}\left(1 + \mathcal{O}(\max\{Ha^{-1}, \alpha^2\})\right), \tag{2.16}$$

where $\alpha = \|\mathbf{u} - \bar{\mathbf{u}}\|/\|\mathbf{u}\|$ represents the degree of three-dimensionality in the flow. For a quasi-two-dimensional flow, $E = E_{2D}(1 + \mathcal{O}(Ha^{-1}))$. We shall see from the analysis of flow profiles in section 5 (figure 6) that in the later stages of the decay, $\alpha \lesssim 0.1$ so E_{2D} can be expected to provide a good approximation for E in the two-dimensional phase of the decay.

The two-dimensional dynamics of the flow is expected to favour the formation of large scales and indeed Schumann (1976) showed that energy transfer towards them occurred during the decay. Areas of strong shear may however persist between them. Furthermore, the typical lengthscale of the viscous core of quasi-two-dimensional MHD is known to scale as $LHa^{-1/2}$ (Sommeria 1988). For such fine quasi-two dimensional structures, Hartmann friction and horizontal viscous friction would be of the same order. For large structures on the other hand, $l_\perp^\nu/L$ should be of the order of unity and so in the limit $Ha \to \infty$, the decay should be strongly dominated by Hartmann friction. The total kinetic energy should then decay as $E \sim \exp(-4t/\tau_H)$. Any discrepancy to exponential decay of this form is therefore the signature either of thin quasi-two-dimensional structures or of a residual three-dimensionality. We shall attempt to measure this discrepancy

in our numerical simulation to identify the mechanisms of the long-term decay. It should, however be noted that for structures such that $l_\perp^\nu/L \sim Ha^{-1/2}$, three-dimensionality subsists anyway because at this scale, friction between horizontal planes balances the diffusion of momentum along the magnetic field.

3. Numerical approach

3.1. *Numerical method*

The problem set out in section 2.1 is solved numerically, using a new type of spectral method designed to alleviate the computational cost associated with strong anisotropy and thin Hartmann boundary layers. Thanks to it, increasing the magnetic field incurs essentially no direct computational cost per time step. The mathematical foundations of this method and numerical implementations are described in detail in Dymkou & Pothérat (2009); Kornet & Pothérat (2014), where it is also tested for the exact channel geometry studied here. For the sake of completeness, we shall nevertheless outline the principle of this new method. Using the spectral approach we seek the solution of eq. (2.6) as the decomposition on elements of basis $\mathbf{u}_i$:

$$\mathbf{u} = \sum_i c_i(t)\mathbf{u}_i(\mathbf{x}). \tag{3.1}$$

As the spatial dependence is carried solely by $\mathbf{u}_i$, when representation (3.1) is injected into eq. (2.6), the latter reduces to the set of ordinary differential equations in time on the unknown coefficients $c_i(t)$ (see Canuto *et al.* (2006) for a detailed description of spectral methods).

For the basis $\mathbf{u}_i$ we choose the set of eigenvalues of the operator $\mathcal{L}$ formally expressed as the right hand side of eq. (2.6), with the electrical and kinematic boundary conditions of the problem. These functions are a natural choice as elements of a functional basis, because the features of flows at high Ha are strongly determined by the properties of this operator. For example they include specific features of the flow such as laminar and turbulent Hartmann boundary layers that develop along the channel walls (Dymkou & Pothérat 2009; Pothérat & Dymkou 2010). Moreover, these modes all have negative eigenvalues, and it can be shown that to resolve the flow completely, it is only necessary to take into account all modes with eigenvalue λ of modulus below a maximum $|\lambda_{\max}|$, such that their total number scales as Re^2/Ha (Pothérat & Alboussière 2006), where Re is the Reynolds number based on the large scales. Since the operator $\mathcal{L}$ represents the sum of viscous and ohmic dissipation, the set of modes defined in this way is in fact the set of *least dissipative modes*.

The main difficulty in solving equation (2.6) using the least dissipative modes lies in calculating the spectral representation of non linear terms $G(\mathbf{u}(x_i, y_i, z_i))$. We use a pseudospectral approach and calculate these terms in real space. Therefore we need a method to reconstruct the spectral coefficients g_n of physical vector fields known at a discrete set of points in space $\mathbf{x}_i$. To this aim we first use the fact that the eigenmodes of $\mathcal{L}$ can be factorised as the product of two scalar functions of x and y respectively, and a vector function of z. Moreover, the functions of x and y consist of Fourier modes, so the set of eigenmodes can be enumerated by a tuple of three numbers (n_x, n_y, n_z) and for every mode we can define the vector function $\mathbf{E}_{n_x,n_y,n_z}(z)$ such that each mode takes the form

$$\mathbf{E}_{n_x,n_y,n_z}(z)\exp\left(ik_{n_x}x + ik_{n_y}y\right). \tag{3.2}$$

Therefore we first calculate the two-dimensional Fast Fourier transform in the x - y directions. This brings the transformed non linear terms under the form:

$$G(\mathbf{u}(x_i, y_i, z_i)) = \sum_{n_x, n_y} \mathbf{A}_{n_x, n_y}(z_i) \exp\left(i2\pi n_x x_i + i2\pi n_y y_i\right), \tag{3.3}$$

where $\mathbf{A}_{n_x,n_y}$ is the complex amplitude of Fourier mode $(2\pi n_x, 2\pi n_y)$. Then, for every value of (n_x, n_y) we find the set of spectral coefficients $\{g_{n_x,n_y,n_z}\}$ by solving a set of equations

$$\sum_{n_z} g_{n_x,n_y,n_z} \mathbf{E}_{n_x n_y n_z}(z_i) = \mathbf{A}_{n_x,n_y}(z_i)\,. \tag{3.4}$$

As the coefficients in this set of equations are constant during a single numerical run, it is worth performing the LU decomposition of the corresponding matrix at the beginning of calculations and later use it to efficiently find the spectral decompositions. Finally the projection onto the subspace of solenoidal vector fields is done by neglecting the coefficients corresponding to modes with non zero divergence. Using the Fast Fourier transform in $x-y$ planes imposes the distribution of discretisation points in these planes: they have to form a regular rectangular grid. We denote its dimensions as $N_x \times N_y$. In our simulations we also use a uniform grid in z direction of dimension N_z. For the set of equations (3.4) to have a unique solution, the number of modes used during the spectral decomposition has to be equal to N_z, and the total number of independent modes used in the calculations is $N = N_x N_y N_z$. The technique described above has the advantage that the obtained spectral decomposition reproduces exactly the physical field on the given set of discretisation points. Therefore momentum and energy are conserved by this procedure. However the spectral coefficients g_n obtained in this way are different from the exact ones $\widetilde{g}_n$, that would be obtained by decomposition of the same vector field over the space of infinite dimension spanned by all eigenvectors of $\mathcal{L}$. $|\widetilde{g}_n - g_n|$ is the so-called aliasing error. To correct this error we adapt the 3/2 technique known from standard spectral methods (Canuto *et al.* 2006). Namely we perform the discrete transformation with additional number of modes N larger than the one strictly required by the system's dynamics, N_D (The latter is of the order of the attractor dimension of the dynamical system underlying the given problem (Pothérat & Alboussière 2006)). After every evaluation of the spectral decomposition, the coefficients corresponding to these additional modes are set to 0.
The spectral method described above was implemented by modifying the spectral code TARANG developed by Verma *et al.* (2013).

3.2. *Simulation strategy*

The bulk of our numerical simulations was based on a domain made of a cube of dimension L divided uniformly into N_x, N_y and N_z cells respectively in x, y and z directions. In order to limit the dealiasing errors we always resolve each of the Hartmann layers with at least three computational cells in the z direction. Our strategy to study the decay of MHD turbulence relies on four different types of simulations, all gathered in table 1. The first type is inspired from the DNS of decaying MHD turbulence in a three-dimensional periodic domain by Okamoto *et al.* (2010): the initial conditions consist of a isotropic, random Gaussian velocity field with $u(k) \sim \exp\left[(-k/k_p)^2\right]$ where $k_p = 4\pi/L$. This corresponds to an energy spectrum $E \sim k^4 \exp\left[-2(k/k_p)^2\right]$. For this choice of initial velocity field, the initial integral scale of turbulent motion is given by $l_0 = \sqrt{2\pi}/k_p$. The velocity spectrum was normalised in such a way that cell sizes in x and y directions correspond to $l_K/1.4$ where $l_K = lRe^{-3/4}$ is the Kolmogorov length scale and the Reynolds number in

its definition $Re = u'l/\nu$ is based on l and velocity $u' = u(k = k_p)$. This strategy allows us to calculate the most intense flow possible whilst minimising mesh-induced numerical errors at a given mesh size, since the mesh is always uniform.

To characterise the influence of the walls, we performed additional simulations starting from exactly the same initial conditions as before, but with periodic boundary conditions imposed in all three directions. For this set of calculations we used a traditional spectral code, TURBO, which uses Fourier modes as the functional basis and was tested and optimised for Low-Rm MHD (Knaepen & Moin 2004; Vorobev *et al.* 2005).

To evaluate a possible influence of the size of the domain in the x and y dimensions, we also performed several simulations with a domain of dimension $2L$ in these directions. These were computationally expensive and therefore run over a shorter period of time than the simulation over a cube of size L.

Finally, The simple order of magnitude analysis from section 2.2 shows that under a strong magnetic field, the decay of MHD turbulence can occurs over a time of the order of a few times τ_J, while a truly quasi-two-dimensional behaviour would not be expected before smaller scales are diffused over the height of the channel, *i.e.* at much later times, of the order of $\tau_H = Ha\tau_J$. Thus, if the initial integral scale l_0 is chosen much smaller than the size of the box, then turbulence will have lost practically all of its kinetic energy by the time the two-dimensional dynamics potentially becomes dominant. This would make it difficult to study the later phase of the decay. On the other hand, l_0/L needs to be sufficiently smaller than unity for a significant three-dimensional phase of the decay to exist and so as to generate a sensible transition between three- and two-dimensional dynamics. To reconcile these antagonistic constraints, we chose $l_0/L = 1/\sqrt{(2\pi)} \simeq 0.4$ and also run additional simulations initialised with the velocity field obtained at $t = 0.5\tau_J, \tau_J$ in the previous simulations, but in which the velocities are renormalised, so that the total energy is restored to its level at $t = 0$. The flow obtained this way is much closer to a quasi-two-dimensional one than the simulations initialised with a random field. Comparing the evolutions of these two different types of initial conditions shall thus give us a good measure of the robustness of the features observed in the later stages of the decay to a change of initial conditions and to the intensity of the initial flow.

4. Three dimensional phase

From the evolution of the total energy (figure 3), the flow progresses in every run through three consecutive phases: during the first one, the flow adjusts from the initial conditions. This phase is very short, (shorter than $0.05\tau_J$ in all cases). In this section, we shall characterise the phase that immediately follows, which features strongly three dimensional turbulence, a fast energy decay and lasts several Joule times. For the time being, the analysis shall be restricted to cubic domains of size L with Hartmann walls, or with periodic boundary conditions when specified. This phase can be identified through the strong three-dimensionality visible in the spatial RMS for all (x, y) of the profile along z of magnitude of $\mathbf{u}_\perp$ on fig. 2. Significant variations along the z direction exist until approximately $t \simeq 1.5 - 2\tau_{2D}(l) \simeq 5 - 10\tau_J$ for all values of Ha This reflects the prominent of the contribution of the large scales to the RMS velocity fluctuations, and confirms that large scales indeed become quasi-two-dimensional in this typical time.

4.1. *Total kinetic energy*

Fig. 3 presents the evolution of the total kinetic energy in this phase for different values of Ha. To compare this evolution to Okamoto *et al.* (2010)'s laws for the decay of un-

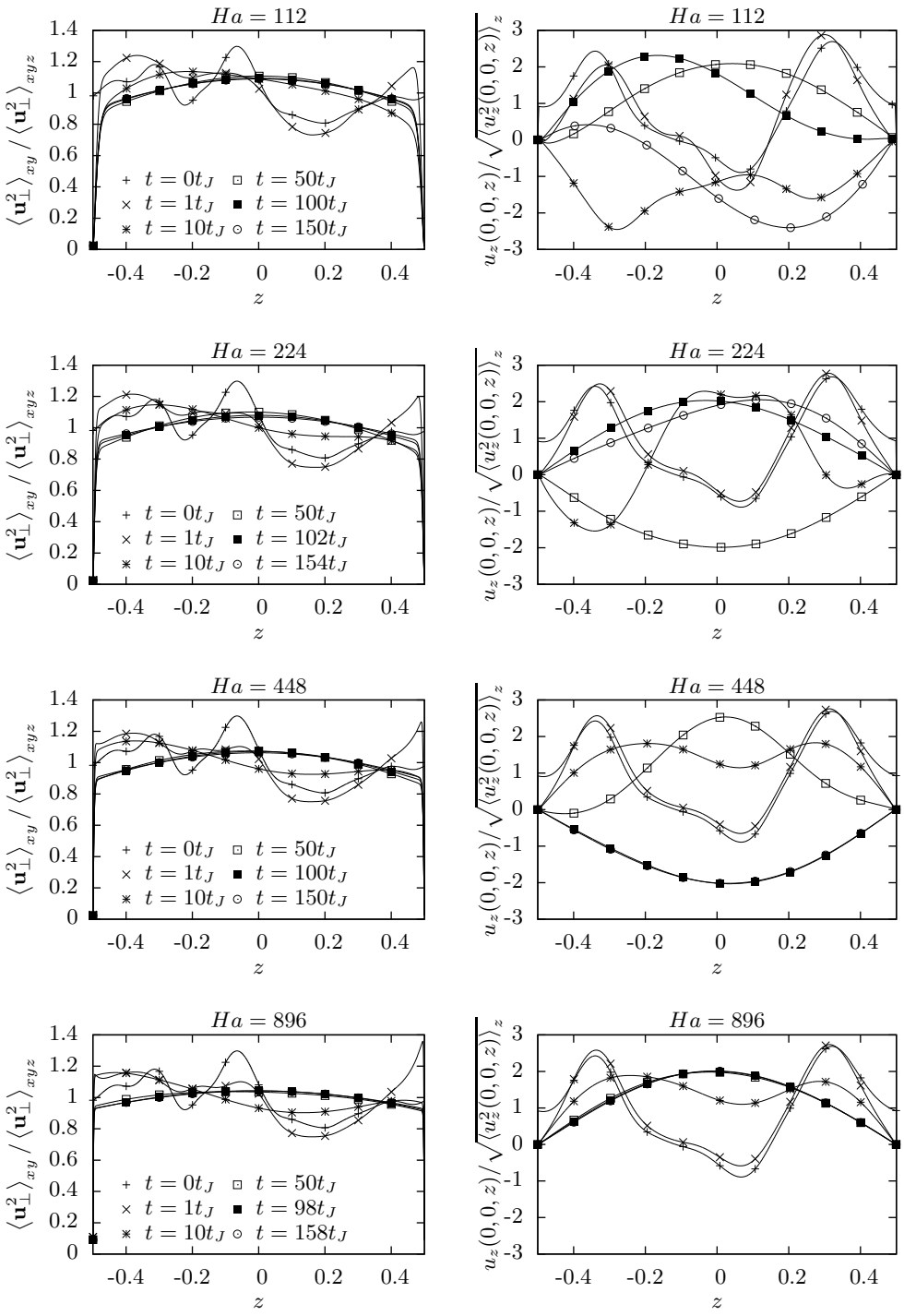


FIGURE 2. Left column: evolution of the normalised, spatial RMS of all vertical profiles of $< \mathbf{u}_\perp^2 >$ over all (x, y) in the domain. Right column: evolution of u_z along a vertical line in the middle of the domain.

Ha	$N_x \times N_y \times N_z$	Boundary conditions in z	$N(t=0)$	$Re(t=0)$	Energy Boost	L_{xy}/L_z
112	$340 \times 340 \times 340$	non slip, insulating	8.55	336	N/A	1
224	$340 \times 340 \times 680$	non slip, insulating	34.2	336	N/A	1
224	$340 \times 340 \times 680$	non slip, insulating	39	261	$t = 0.5\tau_J$	1
224	$340 \times 340 \times 680$	non slip, insulating	43	229	$t = 1\tau_J$	1
448	$340 \times 340 \times 1340$	non slip, insulating	137	336	N/A	1
448	$340 \times 340 \times 1340$	non slip, insulating	161	246	$t = 0.5\tau_J$	1
448	$340 \times 340 \times 1340$	non slip, insulating	170	225	$t = 1\tau_J$	1
448	$680 \times 680 \times 1340$	non slip, insulating	97	238	N/A	2
896	$340 \times 340 \times 1340$	non slip, insulating	548	336	N/A	1
896	$340 \times 340 \times 1340$	non slip, insulating	661	230	$t = 0.5\tau_J$	1
896	$340 \times 340 \times 1340$	non slip, insulating	694	213	$t = 1\tau_J$	1
896	$680 \times 680 \times 1340$	non slip, insulating	387	238	N/A	2
112	$340 \times 340 \times 340$	periodic	8.55	336	N/A	1
224	$340 \times 340 \times 340$	periodic	34.2	336	N/A	1
448	$340 \times 340 \times 340$	periodic	137	336	N/A	1
896	$340 \times 340 \times 340$	periodic	548	336	N/A	1

TABLE 1. Summary of parameters of calculated 3D cases.

bounded, three-dimensional and initially isotropic MHD turbulence, we have fitted the evolution of energy to laws of the form $a(1 + bt)^c$ in ranges from $0.05\tau_J$ to up to $2\tau_J$ (a, b and c are real constants). All values of c are presented in table 2. Okamoto *et al.* (2010) showed that in the limit $N \to \infty$, exponent c should be equal to 1/2. In our cases, we obtain the best fits for $c = 0.95$, 0.75, 0.69 and 0.50 for $Ha = 112$, 224, 448 and 896 respectively, over $[0.05\tau_J, \tau_J]$. This fit is also relatively robust to a variation of the fitting interval, as exponents decrease only slightly when the interval is extended to $[0.05\tau_J, 2\tau_J]$. From this, we infer that the decay of turbulence between walls is in this line with these authors' prediction over a duration of about τ_J. Values of c are however slightly higher for cases with periodic boundary conditions over this interval, which suggests that the influence of the walls is present but moderate for $t \lesssim \tau_J$. This phase corresponds to roughly 25-50% of the time interval where we identified strong three-dimensionality in the profiles of RMS velocity fluctuations (figure 2). From times $t > \tau_J$, by contrast, the kinetic energy tends to decay at a slightly slower rate than predicted by Okamoto *et al.* (2010) in all cases. This is an indication that some of the turbulent structures interact with the walls, as they become stretched vertically under the effect of diffusion by the Lorentz force. The energy of such structures is dissipated partly by the action of eddy currents recirculating in the Hartmann layers. This Hartmann friction mechanism is typically Ha times slower than Joule dissipation, which would be the unique electromagnetic dissipation mechanism if these structures were not in contact with the wall. This explains that the decay of energy slows down for $t \gtrsim \tau_J$.

All cases where the energy was boosted during the three-dimensional phase exhibit a similar behaviour to cases where the energy was left to decay from the start. Nevertheless, for all of them, the value of the c coefficient fitted over intervals of τ_J or more is lower than for their counterpart without energy boost. Furthermore, the later the energy is boosted, the lower the value of c. This slower decay reflects the influence of the anisotropy of the boundary conditions: at the time of the energy boost, the flow recovers the same energy as the initial one but conserves the anisotropy that has developed during the initial decay, before the energy was boosted. Consequently, vortices are more

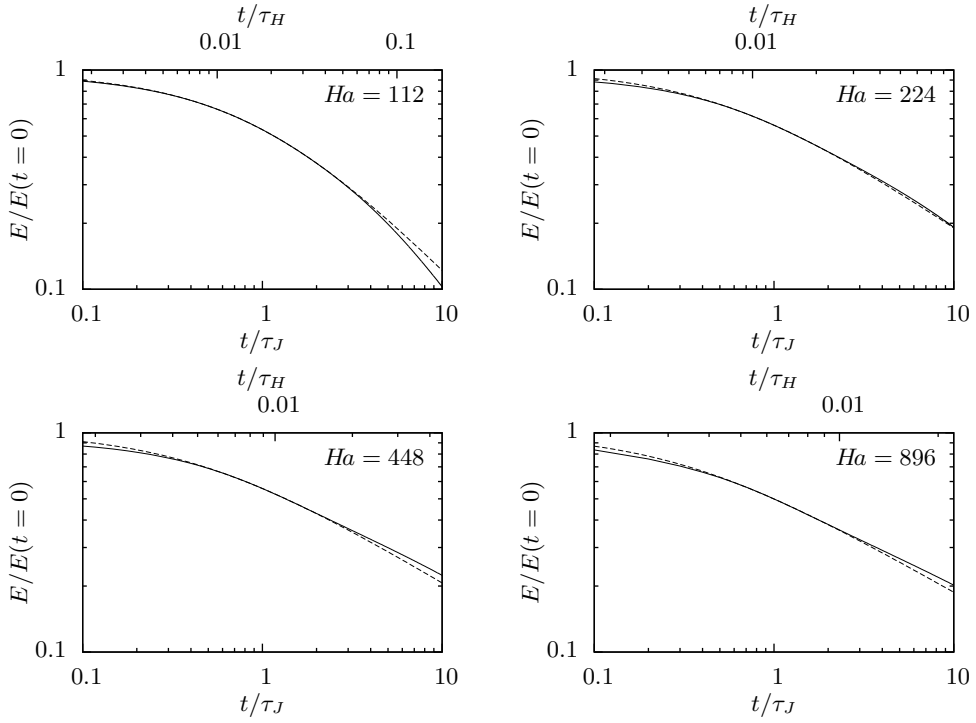


FIGURE 3. Evolution of total kinetic energy, normalised by its value at $t = 0$ (solid line). The dashed line represents the fitted law of the form $a(1 + bt)^c$ over interval $[0.2, 2\tau_J]$.

elongated, interaction with the walls is more significant and the slower friction in the Hartmann layers represents a more important fraction of the dissipation.

4.2. *Dissipation*

Initially, the kinetic energy is mainly dissipated ohmically and the initial ratio of viscous to Joule dissipation scales as $\sim 1/Ha$. As the flow becomes more two-dimensional, both viscous and Joule dissipations diminish in the bulk of the flow (between the Hartmann layers). Conversely, dissipation in the Hartmann boundary layers increases as more and more structures interact with the walls. Therefore, the main contribution from the total dissipation ends up coming from the Hartmann layers (see fig. 4). For $Ha = 112$, 224, 448 and 896 dissipation in the layers becomes larger than in the bulk at $t = 25\tau_J$, $37.6\tau_J$, $45.1\tau_J$ and $54\tau_J$ respectively. However in the Hartmann layers the Joule dissipation is nearly the same as viscous dissipation. Therefore the global ratio of viscous to Joule dissipation increases with time. The value of this ratio becomes larger than unity for $t = 6.3\tau_J$, $19\tau_J$, $50.1\tau_J$ and $88\tau_J$ (or equivalently at $t = 0.056\tau_H$, $0.084\tau_H$, $0.11\tau_H$ and $0.2\tau_H$) for $Ha = 112$, 224, 448 and 896 respectively. In all cases, the ratio ϵ_ν/ϵ_J tends to an asymptotic value of ~ 1.3 after a time of the order of τ_H. From this perspective, the dissipation behaves as in a three-dimensional flow during a period of time that is longer than the timescale of three-dimensional Joule dissipation τ_J, but shorter than that of two-dimensional effects τ_H. This intermediate time scale is an indication that although large scales become two-dimensional over a time of the order of $\tau_{2D}(l)$, smaller scales remain three-dimensional during a significantly longer period of time. After $t > 1.5 - 2\tau_{2D}$, the contribution of the large scales to the total dissipation comes mostly from the Hartmann layer, where it is weak, whereas the contribution of the small scales consists of stronger

		E fitted from $0.05\tau_J$ to				l_z fitted from $0.05\tau_J$ to			
Ha	Remarks	$2\tau_J$	τ_J	$0.5\tau_J$	$0.2\tau_J$	$2\tau_J$	τ_J	$0.5\tau_J$	$0.2\tau_J$
112		-0.91	-0.95	-0.97	-0.86	0.18	0.21	0.24	0.26
224		-0.65	-0.75	-0.82	-0.71	0.26	0.33	0.37	0.42
448		-0.59	-0.69	-0.42	-0.83	0.27	0.34	0.38	0.44
896		-0.51	-0.51	-0.41	-0.34	0.26	0.34	0.37	0.44
224	E boosted at $0.5\tau_J$	-0.54	-0.58	-0.63	-0.68	0.20	0.25	0.28	0.29
448	E boosted at $0.5\tau_J$	-0.46	-0.53	-0.73	unstable	0.20	0.26	0.29	0.40
896	E boosted at $0.5\tau_J$	-0.45	-0.56	unstable	unstable	0.21	0.29	unstable	unstable
224	E boosted at $1\tau_J$	-0.50	-0.51	-0.52	-0.56	0.15	0.20	0.22	0.22
448	E boosted at $1\tau_J$	-0.43	-0.48	-0.70	unstable	0.18	0.23	0.25	0.39
896	E boosted at $1\tau_J$	-0.43	-0.52	unstable	unstable	0.19	0.24	0.36	unstable
112	periodic BC	-0.76	-0.86	-0.96	-1.05	0.33	0.37	0.40	0.42
224	periodic BC	-0.56	-0.69	-0.79	-0.74	0.40	0.50	0.55	0.59
448	periodic BC	-0.52	-0.65	-0.82	-1.02	0.42	0.50	0.56	0.64
896	periodic BC	-0.47	-0.58	-0.66	-0.89	0.43	0.51	0.57	0.65
448	Domain $2L \times 2L \times h$	-0.91	-1.04	-1.14	-1.22	0.38	0.49	0.56	0.66
896	Domain $2L \times 2L \times h$	-0.87	-1.03	-1.29	-1.68	0.37	0.46	0.45	0.38

TABLE 2. Fitted values for constant c in Okamoto *et al.* (2010)'s laws of the form $a(bt+1)^c$ for the decay of total kinetic energy and the growth of integral scale l_z. Cases where the formal error of the least squares method was greater than 20% are marked as "unstable".

Joule dissipation in the bulk. Joule dissipation therefore remains higher than viscous dissipation until this contribution has significantly reduced, which occurs on a timescale of at most τ_H (see section 2.2).

4.3. *Integral lengthscales*

Figure 5 (top) shows the initial evolution of the integral lengthscale in the z direction l_z, and in the direction orthogonal to the magnetic field $l_\perp$. These are respectively defined as:

$$l_z = \frac{\int\int u_z(x,y,z)u_z(x,y,z+z')\,\mathrm{d}V dz'}{\int u_z^2(x,y,z)\,\mathrm{d}V} \tag{4.1}$$

$$l_\perp = \frac{1}{2}\left(\frac{\int\int u_x(x,y,z)\cdot u_x(x+x',y,z)\,\mathrm{d}V dx'}{\int u_x^2(x,y,z)\,\mathrm{d}V} + \frac{\int\int u_y(x,y,z)\cdot u_y(x,y+y',z)\,\mathrm{d}V dy'}{\int u_y^2(x,y,z)\,\mathrm{d}V}\right). \tag{4.2}$$

The initial growth of l_z can be again fitted with the formula $a(1+bt)^c$. Except for $t < 0.2\tau_J$, the fitted value of c is significantly smaller than Okamoto *et al.* (2010)'s theoretical value of 0.5. It is also strongly dependent on the fitting interval for $Ha = 224$, 448 and 896. For $Ha = 112$ the integral lengthscale l_z grows even more slowly with a fitted value down to $c \approx 0.18$ over $[0.05, 2\tau_J]$. This behaviour indicates a very strong influence of the walls on the growth of l_z from the outset of the decay. It is somewhat remarkable that despite this early influence of the walls on l_z, the energy decay shows little influence of the walls during as long as τ_J – $2\tau_J$. During this initial stage l_z also grows faster for larger values of Ha, with indication that at $Ha = 224$, it is already close to its asymptotic behaviour (in the sense of large Ha). For $t \gtrsim 1.5\tau_J$, the growth of l_z

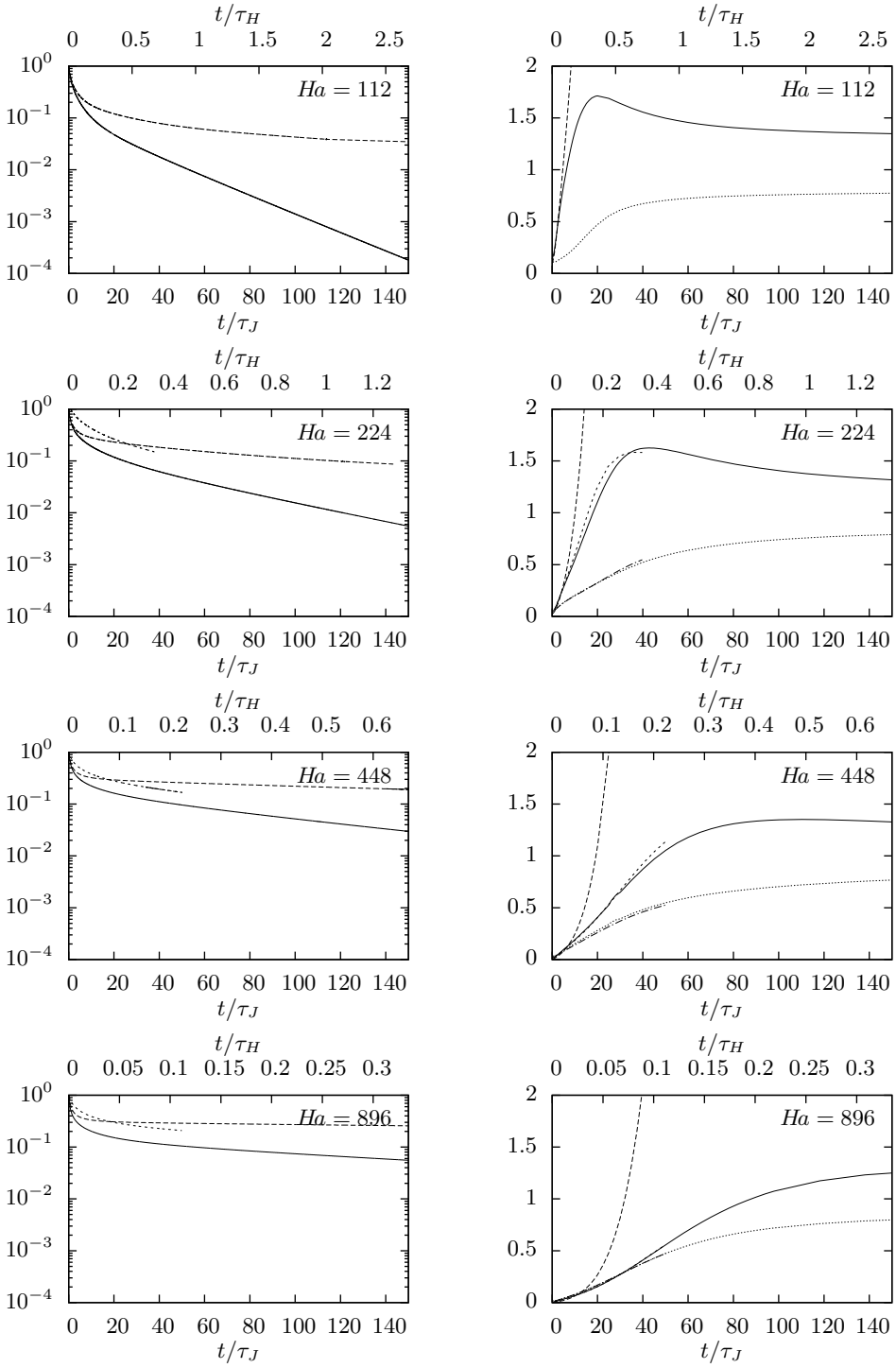


FIGURE 4. Left column: evolution of the kinetic energy in cases with walls (solid lines), periodic boundary conditions (dashed line). Right column: ratio of viscous to Joule dissipation in cases with walls (solid line) and periodic boundary conditions (dashed line). The dotted line represent the fraction of energy which is dissipated in Hartmann layers in cases with wall. On all graphs, the shorter curves represent the case with walls where energy was boosted at $t = 0.5\tau_J$ (Short dashed line: Joule to viscous dissipation, short dash-dotted line: fraction of dissipation in the Hartmann layers) .

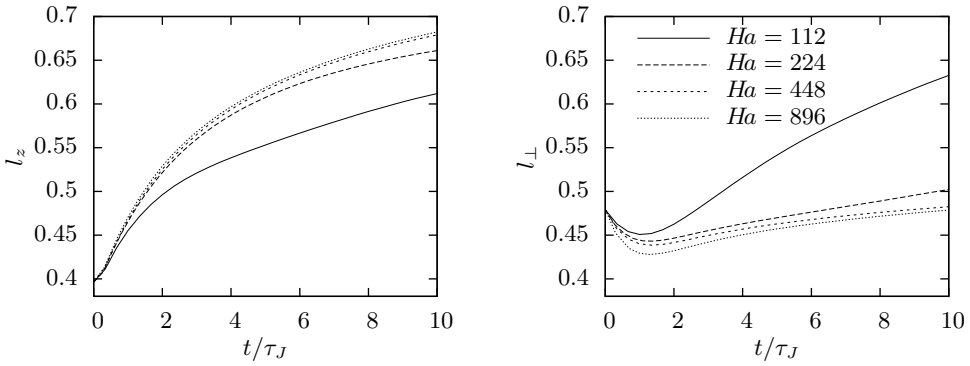


FIGURE 5. Evolution of integral lengthscales l_z (left) and $l_\perp$ (right) in the presence of Hartmann walls.

slows significantly. As for the energy, this is due to the increasingly wide range of scales at which structures reach the walls during the two-dimensionalisation process, and whose growth in thus impeded in the z direction.

With periodic boundary conditions, the fitted value of exponent c is higher than with Hartmann walls. It is close to the theoretical value of 0.5 at high Ha for $t < \tau_J$, and decreases thereafter. Unlike in cases with walls, this behaviour is quite insensitive to the fitting interval for $t < \tau_J$, which confirms the validity to Okamoto *et al.* (2010)'s law at high Ha over at most one Joule time. The validity of this law also indicates that the parameter $l_\perp(t = 0)/L$ was chosen sufficiently small to observe the main features of three-dimensional unbounded turbulence in a periodic domain. However, the fact that this exponent is higher with periodic boundary conditions than with walls suggests that eddy currents circulating between the Hartmann layer and the bulk (when walls are present) strongly increase the influence of the boundaries compared to the periodic case where this effect is absent.

The integral lengthscale $l_\perp$ grows very slowly during the decay. This is consistent with the prediction of Okamoto *et al.* (2010) of a growth as $(t/\tau_J)^{1/7}$. However such a small exponent is difficult to quantify on a timescale of the order of τ_J, where it is expected to be valid. Furthermore, $l_\perp$ evolves slowly all the way through our calculations, with no clear evidence of different behaviour when the flow is close to two-dimensional than when it is three-dimensional.

5. Quasi-two dimensional phase

We shall now describe the later stage of the flow evolution where it approaches a quasi-two dimensional behaviour, and characterise this asymptotic regime.

5.1. *Velocity profiles*

When this stage is reached, the spatial RMS over all (x, y) of the profile along z of $\mathbf{u}_\perp$ have already been considerably smoothed out during the three-dimensional phase of the decay. In every case, we were able to identify a time τ_{Q2D}, from which the profile starts to flatten monotonically without qualitatively changing shape. This type of decay would be expected from a flow governed by mostly two-dimensional dynamics. τ_{Q2D} was defined as the time at which the maximum value in the velocity profile starts decreasing monotonically. It was found at $19.3\tau_J (= 0.34\tau_H)$, $37.6\tau_J (= 0.336\tau_H)$, $65.2\tau_J (= 0.29\tau_H)$ and $98\tau_J (= 0.22\tau_H)$ for $Ha = 112$, 224, 448 and 896 respectively. The fact that it obeys

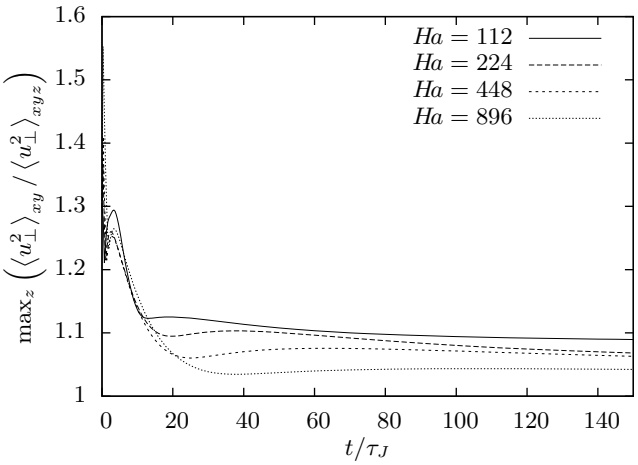


FIGURE 6. Evolution of the maximum of $< \mathbf{u}_\perp^2 >_{xy} / \overline{< \mathbf{u}_\perp^2 >_{xy}}$ (as represented on figure 2).

a timescale of about $0.3\tau_H$ that is commensurate with the two-dimensional timescale τ_H indicates that the large scales only acquire a two-dimensional dynamics once a significant part of the spectrum is close to being two-dimensional (since two-dimensionalisation of the whole spectrum is expected to occur over a period of approximately τ_H). For $t > \tau_{Q2D}$, the evolution of the shape of the profiles is practically unaffected by smaller scales that still retain a three-dimensional behaviour at this stage of the decay.

Remarkably, in none of the cases, did we find that the profile was quasi-two-dimensional after $t \gtrsim \tau_H$ (although such very long times could not be reached for $Ha = 448$). Instead, all profiles seem to have reached a barrel-like shape after $t \sim 50\tau_J$, which evolves only very slowly after this time. Also the shape of the profile is flatter for the larger values of Ha. This shape was first theorised by Pothérat *et al.* (2000) and numerically observed by Mück *et al.* (2000). It stems from eddy currents recirculating between the Hartmann layers and the core. These currents are driven along the axis of columnar vortices. Their leak into the core drives differential rotation between horizontal planes of the vortex leading to the barrel-shaped profile (see also Pothérat (2012)). Since the effect is driven by currents recirculating between the bulk and the Hartmann layer, which scales as Ha^{-1}, it is less marked at high Ha.

The intensity of the barrel effect can be measured through the relative value of the maximum in the profile. The evolution of this quantity is shown on figure 6. First, this graph confirms quantitatively that the barrel effect is less pronounced at higher Ha. Second, the graph also confirms the invariance of the barrel shape of the large scales beyond $t \sim 50\tau_J$. This appears to be verified over at least $100\tau_J$, although the total energy drops by a factor of up to a couple of orders of magnitude during this interval, depending on the value of Ha. This remarkable feature shows that even at high Ha, a form of three-dimensionality subsists a large times, even in the large scales.

Finally, we verified that cases where the energy was boosted at $t = 0.5\tau_J$ and $t = \tau_J$ exhibit the same behaviour, which indicates robustness to initial conditions of this scenario.

5.2. *Energy*

In all calculated cases (with and without energy boost), the evolution of the total kinetic energy in the late phase can be described as an exponential decay with slowly changing

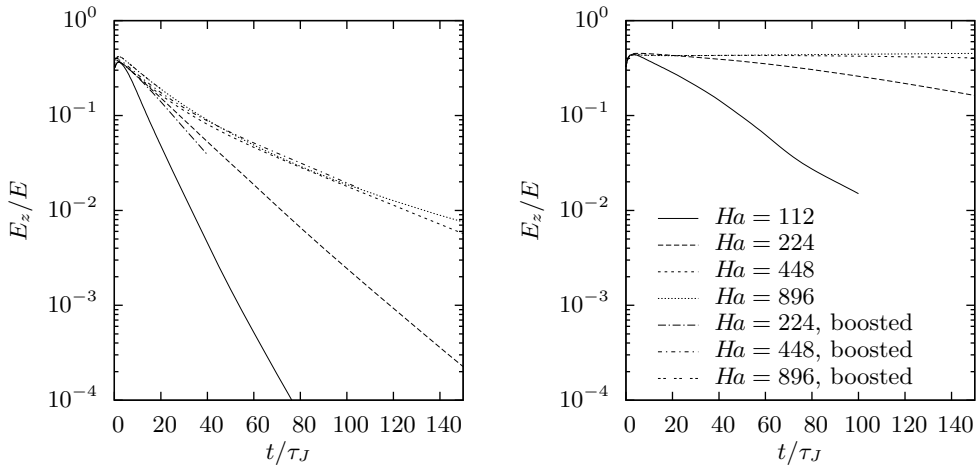


FIGURE 7. Evolution of E_z/E for cases with walls (left) and with periodic boundaries (right).

timescale. However even at the latest time in our calculations this timescale does not seem to converge towards a clear asymptotic value. This indicates that even for $t \gtrsim \tau_H$, when all structures could theoretically be expected to have been diffused across the channel height, the decay is still not entirely dominated by dissipation in the Hartmann layers. The origin of the extra dissipation shall be determined by examining different types of dissipation in section 5.3.

The energy associated to the z component of the velocity is represented on figure 7. For all cases with Hartmann walls, E_z/E tends rapidly to zero, which is consistent with the experimental findings of Kolesnikov & Tsinober (1974) for turbulence in a duct. By contrast, experiments where turbulence was kept far from Hartmann walls (Alemany *et al.* 1979) and simulations with periodic boundary conditions rather than walls (Schumann (1976); Burattini *et al.* (2010)) show a transfer of energy to the velocity component along $\mathbf{B}$, which results in a maximum in E_z/E, followed by a much slower decay than in the case with walls. This supports the explanation put forward by Burattini *et al.* (2010) who hypothesised that the difference between these two scenarii was due to the presence of the Hartmann walls.

The question of how much transport along $\mathbf{B}$ remains asymptotically can be further analysed through the evolution of the skewness coefficient

$$S = \frac{1}{35}\left(\frac{15}{\hat{\epsilon}}\right)^{3/2}\hat{\Gamma}, \tag{5.1}$$

where

$$\hat{\Gamma} = \sum_{\mathbf{k}} 2k^2\hat{\mathbf{q}}(\mathbf{k})\cdot\hat{\mathbf{u}}^*(\mathbf{k}), \tag{5.2}$$

$$\hat{\epsilon} = \sum_{\mathbf{k}} 2k^2\hat{\mathbf{u}}(\mathbf{k})\cdot\hat{\mathbf{u}}^*(\mathbf{k}), \tag{5.3}$$

which Schumann (1976), found to remain constant at large times. This author interpreted this behaviour as an evidence that transport of E_z became important at large times. Our computed evolution of S is shown on figure 8. In the domain with periodic boundary conditions, we recover Schumann (1976)'s findings at high Ha that S seems to converge

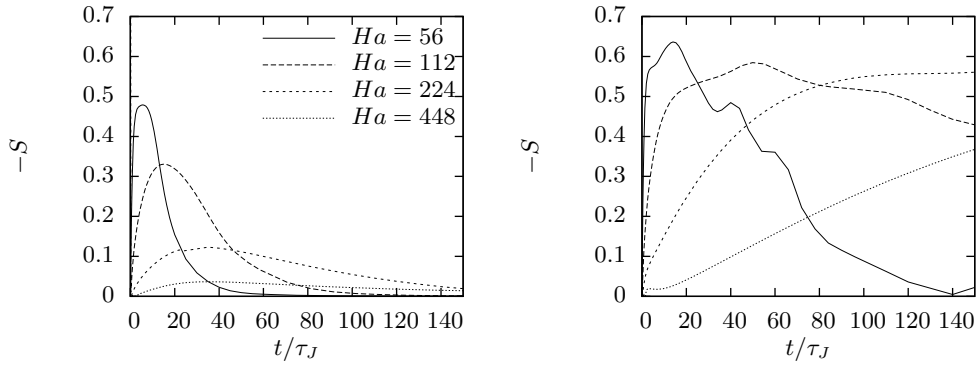


FIGURE 8. Evolution of Skewness S for cases with walls (left) and with periodic boundaries (right).

to a constant asymptotic value. However, as in this authors' work, we were not able to compute S for $t > \tau_H$ at the highest value of Ha, so the two-dimensionalisation process may not be entirely complete at the end of this particular calculation. This leaves room for the possibility that S may in fact evolve on a timescale significantly longer than the duration of our calculations in this case. Simulations with Hartmann walls, by contrast, exhibit a fast decay of S and it is readily visible that $S \to 0$ in all calculated cases. Together with the fast decay of E_z/E, this behaviour confirms that the presence of walls results in a very strong suppression of transport along $\mathbf{B}$, in contrast to the phenomenology of flows with periodic boundary conditions.

Note that in the two-dimensional phase, both E (see fig. 4) and E_z/E appear to decay faster at lower values of Ha in the case with walls. It should however be pointed out that in this phase, turbulence decays over a timescale of $\tau_H = Ha\tau_J$, which appears slower at higher Ha in units of time normalised by τ_J when it is in fact faster in dimensional time units.

Finally, in simulations where the total energy in the flow was artificially boosted at $t = 0.5\tau_J$ (and, we verified, $t = \tau_J$) both E and E_z/E exhibit a similar behaviour to the case without energy boost, which confirms the robustness of this phenomenology to initial conditions.

5.3. *Dissipation*

Asymptotically, the ratio of viscous to ohmic dissipations ϵ_ν/ϵ_J tends to a value of approximately 1.3 for all values of Ha (see fig. 4). For all cases except $Ha = 448$ we observe a maximum in the temporal evolution of this ratio at times $0.35\tau_H, 0.38\tau_H, 0.5\tau_H$ for $Ha = 112$, 224 and 448 respectively. The maximum becomes less pronounced with increasing Ha, with the ratio of maximal value of ϵ_ν/ϵ_J to its asymptotic value decreasing from 1.28 at $Ha = 112$ to 1.04 at $Ha = 448$. We presume that for $Ha = 896$, this maximum is still present for $t \gtrsim 0.5\tau_H$, although even less prominent. This behaviour is very different from that observed in simulations with periodic boundary conditions, where ϵ_ν/ϵ_J increases indefinitely. In both cases the sharp initial increase of this ratio is due to the two-dimensionalisation of smaller and smaller structures. Indeed, from the right hand side of (2.6), the ratio of dissipations for a structure of wavenumber $(k_\perp, \kappa_z)$ is $\epsilon_\nu(k_\perp, \kappa_z)/\epsilon_J(k_\perp, \kappa_z) = Ha^{-2}(1 + (k_\perp/\kappa_z)^2)$. While initially $k_\perp/\kappa_z \sim 1$, $k_\perp/\kappa_z$ becomes very large for nearly two-dimensional structures. As time progresses, this becomes true for increasingly large values of $k_\perp$, and so the ratio of total viscous to Joule dissipations

ϵ_ν/ϵ_J increases. With periodic boundary conditions, strictly two-dimensional structures ($\kappa_z = 0$) can exist and so this ratio is unbounded. In the presence of Hartmann walls, on the other hand, quasi-two-dimensional structures generate little dissipation in the bulk. Most of their dissipation comes from the Hartmann layers, where viscous and Joule dissipation are locally of the same order. This explains that the ratio ϵ_ν/ϵ_J converges to a value of the order of unity.

The presence of the maximum in the evolution of ϵ_ν/ϵ_J at lower values of Ha may be attributed to structures that are too small for magnetic diffusion to stretch them up to the walls, i.e. for which at $t = 0$, $l_z^N(k_\perp) = k_\perp^{-1} N(k_\perp)^{1/2} < L$. These initially generate a large contribution to the ratio ϵ_ν/ϵ_J over a time scale of the order of $\tau_{2D}(k_\perp)$, which is longer than the two-dimensionalisation time of the large scales $\tau_{2D}(l_0)$ but shorter than the decay time of quasi-two-dimensional structures τ_H. For $t \sim \tau_H$, these structures have lost most of their energy and the surviving structures extend across the whole channel. As Ha increases, structures that remain three-dimensional during their entire life span are confined to a region of the spectrum of higher and higher lengthscale and their contribution to the total dissipation progressively vanishes. This explains that the maximum is less pronounced at higher values of Ha, and also that it take place at later times.

More details on the asymptotic state can be obtained by inspecting the ratio of the total dissipation coming from the Hartmann layers to that coming from the bulk (figure 4). Asymptotically, the dissipation comes dominantly from Hartmann layers because the flow becomes close to quasi-two dimensional at all values of Ha investigated here. However, approximately 20% of the dissipation still takes place in the bulk asymptotically. It is tempting to check whether the residual three-dimensionality due to the Barrel effect noted on the velocity profiles (section 5.1) is responsible for this extra dissipation: since it is driven by currents in the Hartmann layers that recirculate in the bulk, Joule dissipation must be associated to it. Current conservation implies that the current densities in the bulk J^C and the Hartmann layers J^H must satisfy $J^H/J^C \sim Ha$ and so the contributions to Joule dissipation from the core and the Hartmann layers must be in a ratio of $\epsilon_J^H/\epsilon_J^C \sim Ha$. This scaling is insufficient to explain the relatively high level of dissipation observed in the bulk: this discards the barrel effect as the residual source of dissipation. To find out the origin of this extra dissipation, we calculated non-dimensional quantity $2Ha^{-1}(L/l_\perp^\nu)^2$, which, from (2.15), represents the actual ratio of quasi-two-dimensional viscous friction to Hartmann friction. It turns out that this ratio converges towards a constant value around 0.2 regardless of the case considered (see figure 10). This implies that extra dissipation in the bulk results from viscous friction incurred by gradients of the x and y components of the velocity in the x and y directions. This extra dissipation also explains that the energy does not decay exponentially even for $t \gtrsim \tau_H$, as would be expected if Hartmann friction was the exclusive dissipation mechanisms. Interestingly, the ratio $2Ha^{-1}(L/l_\perp^\nu)^2$ behaves in roughly the same way whether Hartmann walls are present or not. Even though Hartmann friction is absent when boundary conditions are periodic in all three spatial directions, this ratio still gives a normalised measure of the level of two-dimensional viscous dissipation, which appears to be the same with and without Hartmann walls. Furthermore, our simulations show that in the Hartmann layers, Joule and viscous dissipations are asymptotically the same up to few percent. Therefore viscous dissipation due to horizontal velocity gradients also explains that the ratio ϵ_ν/ϵ_J remains greater than unity even for $t \gtrsim \tau_H$, when two-dimensionalisation is expected be complete over the whole spectrum of lengthscales.

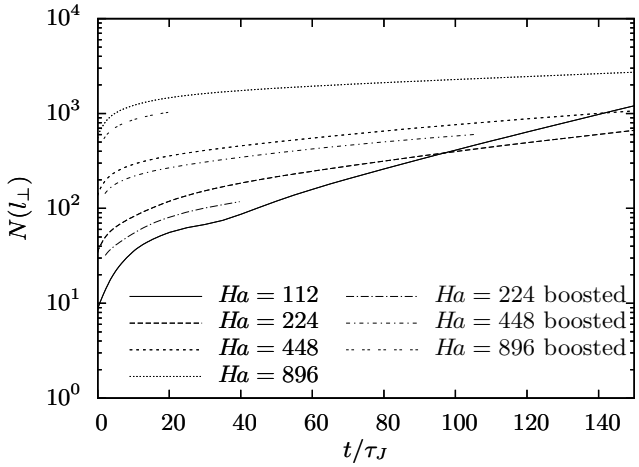


FIGURE 9. Evolution of interaction parameter $N = Bl_\perp/u$,

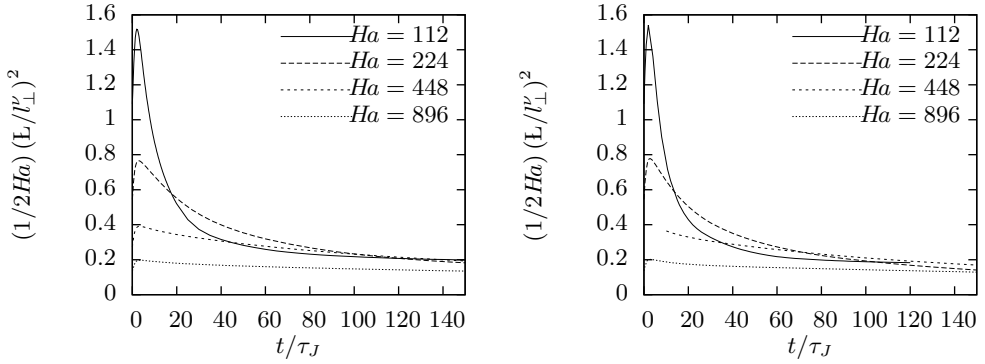


FIGURE 10. Ratio of effective dissipation by two-dimensional viscous friction to Hartmann friction: case with Hartmann wall (left) and case with periodic boundary conditions (right). With periodic conditions, this quantity represents the normalised two-dimensional dissipation only, as Hartmann friction is absent.

5.4. *Integral lengthscales*

Figure 11 shows the evolution of l_z up to the later stages where $t > \tau_H$. For large values of Ha, l_z tends asymptotically to a value of approximately 0.8. By contrast, in simulations with periodic boundary conditions l_z asymptotically tends to 1. At high Ha the Hartmann layers are laminar and not affected by inertia present in the core. The classical theory for these layers then implies that the velocity normal to the wall in the layer is $\mathcal{O}(Ha^{-1})$ and this imposes a region of very low values of u_z near the walls. By contrast, residual velocity may exist in the core and so the z-component of the velocity cannot be correlated over the entire width of the channel (see profiles of vertical velocity on figure 2). This effect is absent with periodic boundary conditions where a constant through-flow can exist in the z-direction, which allows values of l_z close to 1.

The convergence of l_z for cases bounded by walls becomes less smooth for lower values of Ha. For $Ha = 112$, l_z shows no signs of convergence to a finite value. It starts decreasing around $t \sim 45\tau_J$ and still decreases at $t \simeq 3\tau_H$. This behaviour is caused by Ekman pumping in large quasi-two dimensional vortices. This effect tends to produce vertical

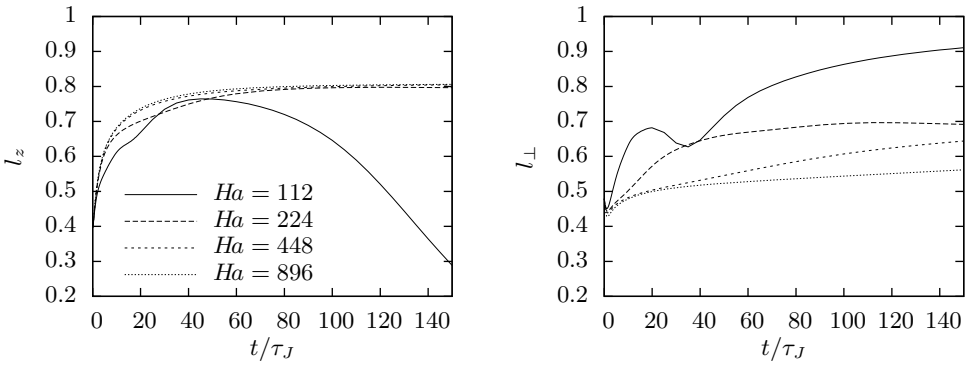


FIGURE 11. Evolution of integral lengthscales l_z (left) and $l_\perp$ (right) for the simulation with walls.

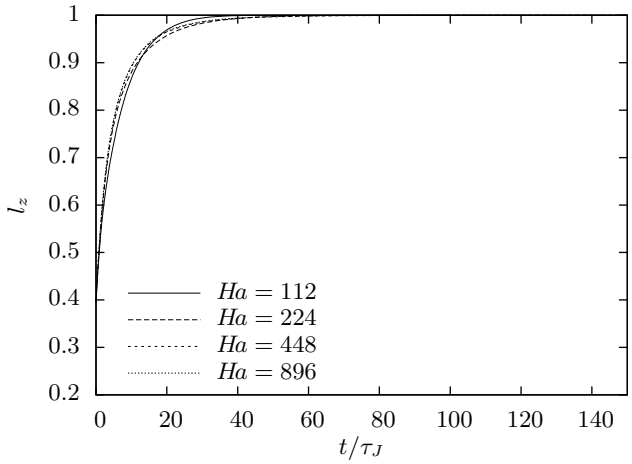


FIGURE 12. Evolution of integral lengthscale l_z for periodic cases.

profiles of u_z that are antisymmetric with respect to the midplane. According to (4.2), reduces the value of l_z as its definition is based on $u_z(z)$ (see fig. 2). The intensity of Ekman pumping is driven by inertia but damped by the Lorentz force: Pothérat *et al.* (2000) showed that it scaled as $u_z/u_\perp \sim Ha^{-2}N^{-1}$. This explains that this effect is only noticeable at the lowest value of Ha. This also suggests that ultimately, since the interaction parameter $N(t)$ diverges asymptotically (see figure 9), Ekman pumping should progressively disappear and l_z may increase again. The evolution of l_z on figure 11 however implies that this may only take place after a very long time, beyond the reach of our calculations. Also, since E_z/E is very small in the later stages of the decay, l_z relies in fact on low values of u_z and only reflects a weak component of the flow, from the Energy point of view. Despite its relative weakness, Ekman pumping is responsible for the larger values of $l_\perp$ at $Ha = 224$ and more noticeably at $Ha = 112$ (figure 11). Ekman pumping indeed transports momentum radially outward of large structure thus increasing their effective size in the horizontal plane (Sommeria 1988).

From this phenomenology, l_z appears dominated by the dynamics of secondary flows but does not reflect accurately the dimensionality of turbulence. We argue that this calls for a more suitable quantity to characterise the growth of vertical scales along the z

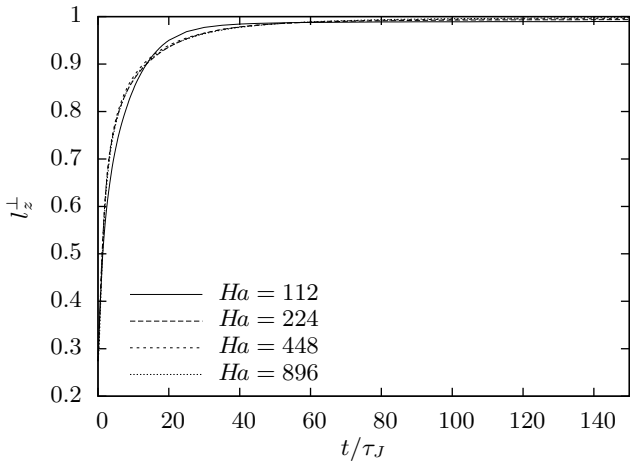


FIGURE 13. Evolution of integral lengthscale $l_z^\perp$ for simulations with walls.

direction. We propose that such a quantity may be defined as:

$$l_z^\perp = \frac{\int\int \mathbf{u}_\perp(x,y,z)\mathbf{u}_\perp(x,y,z+z')\,\mathrm{d}V dz'}{\int u_\perp^2(x,y,z)\,\mathrm{d}V}\,. \tag{5.4}$$

The temporal evolution of $l_z^\perp$ is shown on fig. 13 for decaying turbulence between walls. In contrast to l_z it asymptotically converges to 1 for all values of Ha and curves remain very close to each other in all stages of the evolution. During the initial stage, $l_z^\perp$ grows over a time scale of $\tau_{2D}(l)$, which does reflect the two-dimensionalisation of the large scales. $l_z^\perp$ reaches a value of 0.9 at $\sim 15\tau_J$ for all values of Ha, and its subsequent evolution in the quasi-two-dimensional phase is only slow. This indicates $l_z^\perp$ is only weakly affected by the two-dimensionalisation of smaller scales, unlike the total kinetic energy and the dissipation.

6. Robustness analysis

In order to focus on the long term evolution of the decay of turbulence and still keep computational costs reasonable, we have conducted our study with a domain of limited size and used only one set of isotropic initial conditions. Ongoing experiments on decaying turbulence conducted on the FLOWCUBE setup (Pothérat & Klein (2014)) show that reliable quantitative laws require ensemble averaging on a large number of initial conditions, which cannot be done numerically. Nevertheless, we shall now estimate the impact of these choices on the mechanisms found, by examining the result of two simulations in a channel four times bigger (dimensions $2L\times 2L\times L$), with different random initial conditions (albeit with the same statistical properties as in the cases where energy has not been boosted), and slightly smaller initial Reynolds number (see table 1).

Comparison between energy decay and dissipation ratios in small and large domains is shown on figure 14. The decay follows a similar profile in both cases. In the three-dimensional phase, fits to Okamoto *et al.* (2010)'s decay laws yields exponents that are consistently higher in the case of a larger domain. Nevertheless their variations with Ha and with the fitting interval are consistent between cases (see table 2). We also noticed that actual values of the exponent are sensitive to the lower bound of the fitting interval, but that again, variations with Ha and with the fitting interval are consistent between

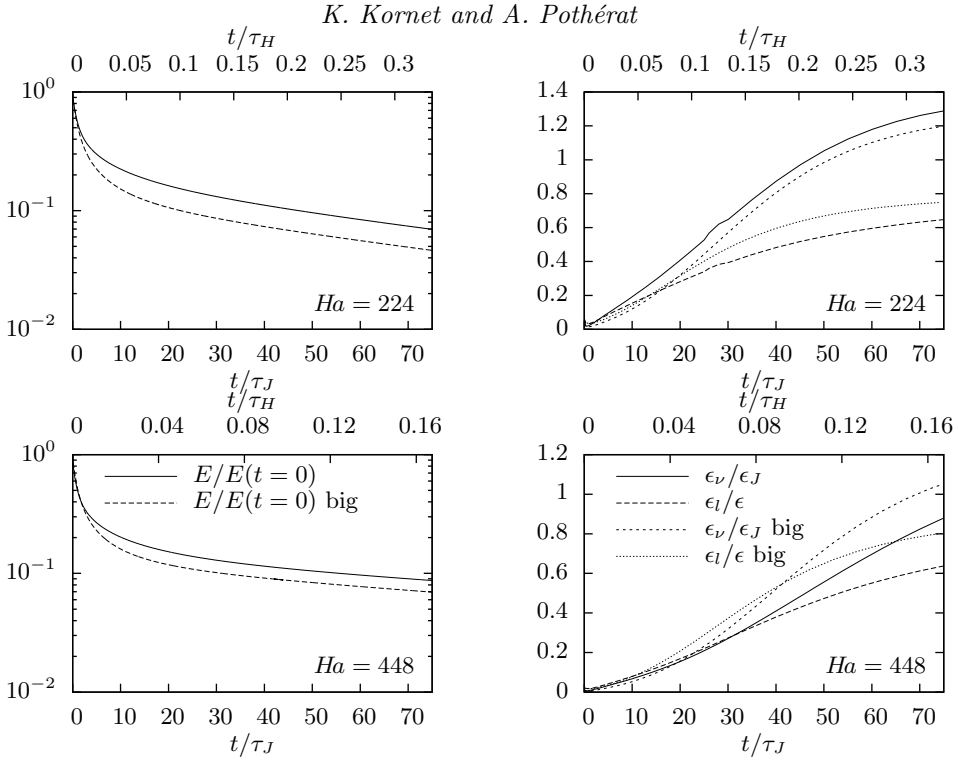


FIGURE 14. Evolution of energy (left) and dissipation rates (right) in smaller and larger domains (marked "big" in the legend), with Hartmann walls.

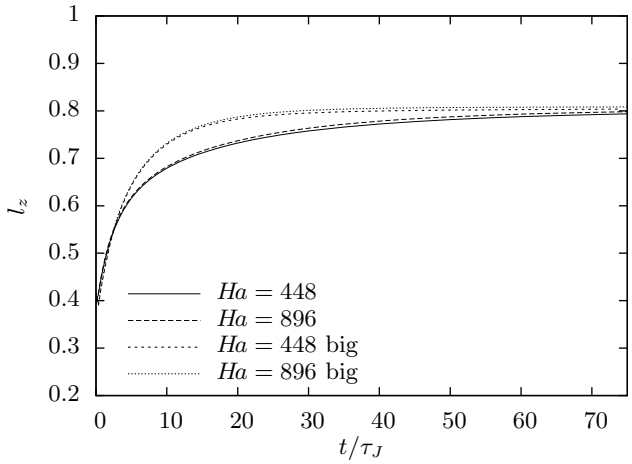


FIGURE 15. Evolution of l_z in smaller and larger domains (marked "big" in the legend) with Hartmann walls

cases, for the same lower bound. This sensitivity can most likely be attributed to the lack of an ensemble average which, as in experiments, would be required for a precise estimate of exponents in Okamoto *et al.* (2010)'s decay laws.

Nevertheless, the interval of validity of the these laws, can still be estimated by varying the upper bound of the fitting interval, and this yields consistent results between cases

and choices of fitting interval. Most importantly, the main properties of the decay outlined throughout the paper appear consistent between the two sets of simulations: the duration of the three-dimensional phase is of the order of $\tau_{2D}(l_0)$ in both cases, and the asymptotic behaviours are identical as decays of energy are parallel to each other. Similarly, Ratios of dissipations (dissipation in the Hartmann layer to dissipation in the bulk and viscous to Joule dissipation), depict the same phenomenology as the evolution of energy: timescales are identical for both domains and evolution curves are parallel. The integral lengthscale (figure 15) too evolves initially in a similar fashion in both cases and converges to the same asymptotic value. In conclusion to this short analysis, although it is difficult to precisely verify the numerical value of the exponents predicted in Okamoto *et al.* (2010)'s laws, the scenario for the decay outlined through the analysis cubic domain seems robust to changes in numerical parameters.

7. Conclusion

Using a new type of spectral methods based on the least dissipative eigenmodes of the dissipation operator, we were able to perform direct numerical simulations of freely decaying turbulence in a strong magnetic field, between two Hartmann walls. The decay exhibits three- and a two-dimensional phases with an overlap: the former is dominated by the two-dimensionalisation process, where diffusion by the Lorentz force stretches vortices until they reach the Hartmann walls. This process is highly dissipative and leads to a rapid variation of energy and of the integral lengthscale along $\mathbf{B}$. Larger scales are two-dimensionalised more quickly than smaller ones. Once the large scales of turbulence are close to two-dimensional (after $\tau_{2D}(l_0)$) the flow starts exhibiting a two-dimensional dynamics, where dissipation mostly takes place in the Hartmann boundary layers, with a slower characteristic timescale $\tau_H = Ha\tau_J$. However since it can take up to τ_H for small scales to adopt a two-dimensional dynamics, there is no clear separation between these two phases and both two and three-dimensional dissipation mechanisms co-exist long after $\tau_{2D}(l_0)$. We were able to single out several important features of this phenomenology: First, the presence of the walls turned out to impede the growth of l_z right from the earliest stages of the decay, whereas the decay of energy remained roughly in line with Okamoto *et al.* (2010)'s law of $E \sim t^{-1/2}$ for unbounded turbulence in the limit of high Ha, during around one Joule time.

Second, energy associated to the velocity component across the channel is very strongly suppressed: E_z/E tends to 0 much faster than for unbounded turbulence. This result is consistent with Kolesnikov & Tsinober (1974)'s experiments and confirms Burattini *et al.* (2010)'s hypothesis that the presence of walls is responsible for the suppression of the third component. Further evidence of this suppression is visible in the long term behaviour of the skewness which tends to 0 in the case with walls. With periodic boundary conditions, by contrast, the Skewness apparently tends to a constant value. However, this only seems true at high Ha. Since, two-dimensionalisation occurs over a timescale of the order of τ_H which is much longer than our calculations at high Ha, and than calculations in previous studies, it is unclear whether the Skewness indeed remains constant past the two-dimensional phase with periodic boundaries.

Long into the "two-dimensional phase", we found that even at the highest value of Ha, a form of three-dimensionality subsisted, due to currents recirculating between the Hartmann layers and the bulk. This effect is characterised by the barrel shape visible on the larger structures, as predicted by Pothérat *et al.* (2000). Though less pronounced at higher values of Ha, our simulations show no evidence of it vanishing at larger times.

Thirdly, in quasi-two dimensional flows dominated by dissipation in the Hartmann bound-

ary layers, the total kinetic energy would be expected to decay exponentially with a timescale of τ_H. However, a true exponential decay of this sort was never observed, even for $t \gtrsim \tau_H$. Remarkably this discrepancy to a pure exponential decay did not result from the residual three-dimensionality due to the barrel effect, but mostly from viscous friction in the horizontal plane.

Finally, at more moderate values of Ha ($Ha = 112$), secondary flows in large structures significantly affect the decay by increasing the integral lengthscale in the directions along the channel (perpendicular to $\mathbf{B}$). Since, however this effect is driven by two-dimensional inertia, it is expected to vanish at larger times, but was still present after $2.5\tau_H$. When present, it is shown to dominate the behaviour of the integral lengthscale in the direction of the magnetic field. This prompted us to put forward an alternative definition for this integral lengthscale that gives a better measure of the flow dimensionality.

The authors are grateful to the Leverhulme Trust, who supported this work through Research Project Grant ref. F00/732J and to Professor Mahendra K. Verma, who made his Fourrier-base spectral code available to them as a basis for the implementation of their novel spectral method.

REFERENCES

Alemany, A., Moreau, R., Sulem, P. & Frish, U. 1979 Influence of an external magnetic field on homogeneous mhd turbulence. *Journal de Mécanique* **18** (2), 277–313.

Baker, N., Pothérat, A. & Davoust, L. 2015 Three-dimensional stucture of electrically driven vortices, the. *J. Fluid Mech., Submitted* .

Burattini, P., Zikanov, O. & Knaepen, B. 2010 Decay of magnetohydrodynamic turbulence at low magnetic reynolds number. *J. Fluid Mech.* **657**, 502–538.

Canuto, C., Hussaini, M. Y., Quarteroni, A. & Zang, T. A. 2006 *Spectral Methods: Fundamentals in Single Domains*. Springer-Verlag.

Dymkou, V. & Pothérat, A. 2009 Spectral methods based on the least dissipative modes for wall-bounded mhd turbulence. *J. Theor. Comp. Fluid Mech.* **23** (6), 535–555.

Knaepen, B. & Moin, P. 2004 Large-eddy simulation of conductive flows at low magnetic reynolds number. *Phys. Fluids* **16** (5), 1255–1261.

Kolesnikov, Y. B. & Tsinober, A. B. 1974 Experimental investigation of two-dimensional turbulence behind a grid. *Fluid Dyn.* **9** (4), 621–624.

Kornet, K. & Pothérat, A. 2014 Spectral methods based on the least dissipative modes for wall bounded mhd flows. *J. Comp. Phys.* pp. submitted, arXiv:1403.4129.

Moffatt, H. K. 1967 On the suppression of turbulence by a uniform magnetic field. *J. Fluid Mech.* **28**, 571–592.

Moreau, R. 1990 *Magnetohydrodynamics*. Kluwer Academic Publisher.

Mück, B., Günter, C. & Bühler, L. 2000 Buoyant three-dimensional mhd flows in rectangular ducts with internal obstacles. *J. Fluid Mech.* **418**, 265–295.

Okamoto, N., Davidson, P. A. & Y. Kaneda, Y 2010 On the decay of low-magnetic-reynolds-number turbulence in an imposed magnetic field. *J. Fluid Mech.* **651**, 295–318.

Pothérat, A. 2012 Three-dimensionality in quasi-two dimensional flows: Recirculations and "barrel" effets. *EPL (Europhys. Lett.)* **98** (6), 64003.

Pothérat, A. & Alboussière, T. 2006 Bounds on the attractor dimension for low-rm wall-bound mhd turbulence. *Phys. Fluids* **18** (12), 25102 (12 pages).

Pothérat, A. & Dymkou, V. 2010 Dns of low-rm mhd turbulence based on the least dissipative modes. *J. Fluid Mech.* **655**, 174–197.

Pothérat, A. & Klein, R. 2014 Why, how and when mhd turbulence at low rm becomes three-dimensional. *J. Fluid Mech.* **761**, 168–205.

Pothérat, A, Rubiconi, F, Charles, Y. & Dousset, V 2013 Direct and inverse pumping in flows with homogenenous and non-homogenous swirl. *EPJ E* **36** (8), 94.

Pothérat, A., Sommeria, J. & Moreau, R. 2000 An effective two-dimensional model for mhd flows with transverse magnetic field. *J. Fluid Mech.* **424**, 75–100.

Roberts, P. H. 1967 *Introduction to Magnetohydrodynamics*. Longmans.

Schumann, U. 1976 Numerical simulation of the transition from three- to two-dimensional turbulence under a uniform magnetic field. *J. Fluid Mech.* **74**, 31–58.

Sommeria, J. 1988 Electrically driven vortices in a strong magnetic field. *J. Fluid Mech.* **189**, 553–569.

Sommeria, J. & Moreau, R. 1982 Why, how and when mhd turbulence becomes two-dimensional. *J. Fluid Mech.* **118**, 507–518.

Verma, M. K., Chatterjee, A., Reddy, S., Yadav, R., Paul, S., Chandra, M. & Samtaney, R 2013 Benchmarking and scaling stuides of pseudo-spectral code tarang for turbulence simulations. *PRAMANA J. Phys.* **81** (4), 617–629.

Vorobev, A., Zikanov, O., Davidson, P. A. & Knaepen, B. 2005 Anisotropy of magnetohydrodynamic turbulence at low magnetic reynolds number. *Phys. Fluids* (17), 125105.